ISAR-8 [R4-P05]
@Tama-Mirai-Messe, Tokyo
October 29, 2025

Decadal surface energy and mass balance variations observed around the equilibrium line altitude in Qaanaaq Ice Cap, northwest Greenland, during 2012–2022

Motoshi Nishimura[1], Teruo Aoki[2], Masashi Niwano[2], Motomu Oyama[3], Sumito Matoba[4], Tomonori Tanikawa[2], Satoru Yamaguchi[5], Rigen Shimada[6], and Takumi Suzuki[6]

[1]Institute for Mountain Science, Shinshu University, [2]Meteorological Research Institute, Japan Meteorological Agency, [3]Graduate School of Engineering, Kogakuin University, [4]Institute of Low Temperature Science, Hokkaido University, [5]Snow and Ice Research Center, National Research Institute for Earth Science and Disaster Resilience, [6]Japan Aerospace Exploration Agency, Earth Observation Research Center

Contact: nishimura.motoshi@shinshu-u.ac.jp

INTRODUCTION

Recent global warming has resulted in notable environmental changes within the cryosphere. Accelerated glacier mass loss is particularly pronounced in relatively low-elevation areas, such as the coastal and peripheral glaciers in Greenland (e.g., Noël et al., 2017) and the northwest region (e.g., Mouginot et al., 2019).

In this context, Tsutaki et al. (2017) and Sugiyama et al. (2021) indicated that the equilibrium line altitude (ELA) of there was situated within an elevation zone between 700 and 1000 m a.s.l. using stake observation. Based on these studies, it was possible to confirm that the SIGMA-B site is situated just above the ELA of the Qaanaaq Ice Cap.

The annual ELA varies significantly from year to year means that the area around the ELA is exposed or not exposed to the ice surface, meaning that the surface energy balance (SEB) near the ELA is controlled by intense changes in the surface (albedo) and atmospheric conditions.

In this study, we focus on the interannual variations over a decade in the SEB and SMB near the ELA of the Qaanaaq Ice Cap in northwest Greenland and the controlling factors of these variations (in particular, albedo, clouds, and radiation). We quantitatively clarified the mechanisms of the annual variations in the SEB and SMB.

ABSTRACT

Study objective:

Revealing the interannual variations over a decade in the SEB, SMB, and controlling factors of those at the SIGMA-B site, near the ELA of the Qaanaaq Ice Cap in northwest Greenland

– This study presents the SEB and SMB variations during 2012–2022 at the SIGMA-B site, around the ELA in Qaanaaq Ice Cap, northwest Greenland using SEB and the surface height change method (SHM) based on in situ observation meteorological data.
– Results revealed that the most significant surface melt occurred in the summers of 2019 (1058 (SEB) and 1191 (SHM) mm w.e. a^{-1}), and 2015 (974 (SEB) and 731 (SHM) mm w.e. a^{-1}).
– The primary energy contributing to the surface melt in 2014/15 was net shortwave radiation caused by snow/ice albedo feedback, whereas, in 2018/19, it was not only shortwave radiation but also increased downward longwave radiation from the warm cloud cover.
– The accumulative SMB over a decade from 2012 was slightly positive, with a value of +0.26 (SEB) and +0.28 (SHM) m w.e.

CONCLUDING REMARK and OUTLOOK

Exposure of ice surfaces induces large mass loss due to a significant albedo decrease. The ice surface exposure is likely to occur with greater frequency with global warming, the more significant surface mass loss can be expected, as observed in 2015 and 2019 at the SIGMA-B site.

RESULT

Evaluation of surface energy and mass balance models

The root mean square errors (RMSEs) of observed and calculated surface temperatures were 2.57 and 1.48, respectively, for hourly and daily data (Fig. 1a). The coefficients of determination (R^2) between the observed and calculated SMB values were 0.81 (SEB) and 0.47 (SHM), and the RMSEs were 0.28 (SEB) and 0.31 (SHM) m w.e. (Fig. 1b). These results suggest that the SEB model is sufficiently accurate on a daily time resolution, and SMB values calculated using the SEB method were more accurate than those calculated using the SHM.

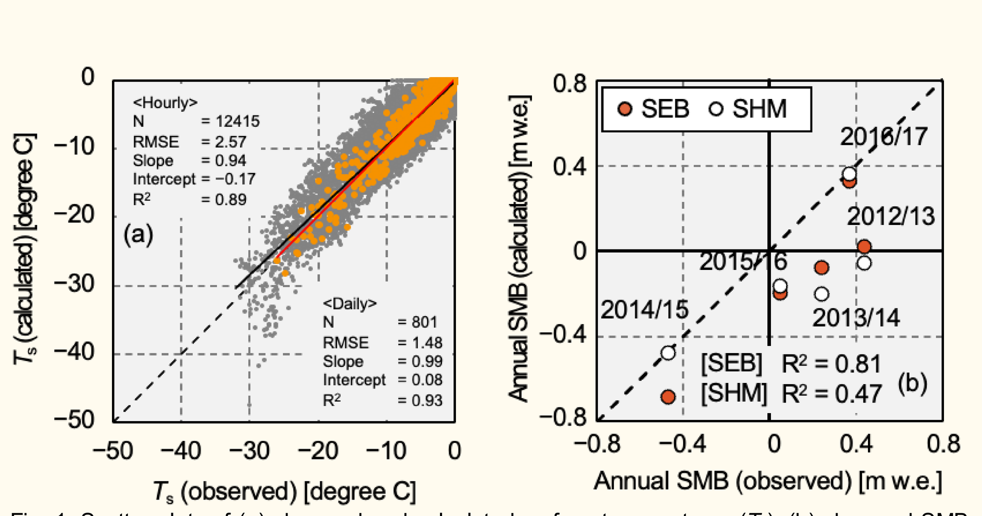

Fig. 1. Scatter plots of (a) observed and calculated surface temperatures (T_s); (b) observed SMB with the stake measurement in Tsutaki et al. (2017) and the calculated SMB_{SEB} and SMB_{SHM} in this study. The data plots for the hourly and daily time steps were colored gray and orange, respectively, and the regression lines were solid black and red in Fig. 1(a).

Surface mass balance variation

Significantly small annual accumulations were observed in 2014/15 (404 mm w.e.) and 2018/19 (452 mm w.e.). The largest ablation amounts ($RU + SU_s + ER_{ds}$) were observed in 2018/19 (SEB: 1075; SHM: 1191 [mm w.e.]). The larger negative annual SMBs were calculated with a combination of small accumulation and large ablation, which occurred in 2014/15 (SMB_{SEB}: −692; SMB_{SHM}: −443 [mm w.e.]) and 2018/19 (SMB_{SEB}: −623; SMB_{SHM}: −739 [mm w.e.]). Figure 6 demonstrates that the SMB over the entire observation period is slightly positive with interannual SMB fluctuations. The cumulative SMBs in August 2022 were +0.26 (SEB) and +0.28 m w.e. (SHM), resulting in a difference of 0.02 m w.e.

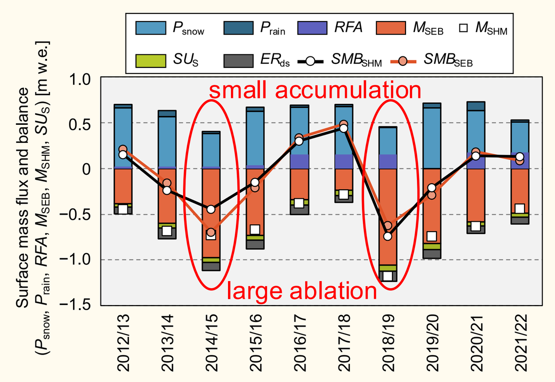

Fig. 5. Temporal variation in annual accumulative amounts of accumulation (P_{snow} and P_{rain}; blue bars), refreezing amount (*RFA*; purple bars), surface melt amount (M_{SEB} and M_{SHM}; red bar and white box plot, respectively), water vapor flux (SU_s; green bar), snow mass flux triggered by wind erosion (ER_{ds}; gray bar), and surface mass balance (SMB_{SEB} and SMB_{SHM}; orange and white circle plots, respectively).

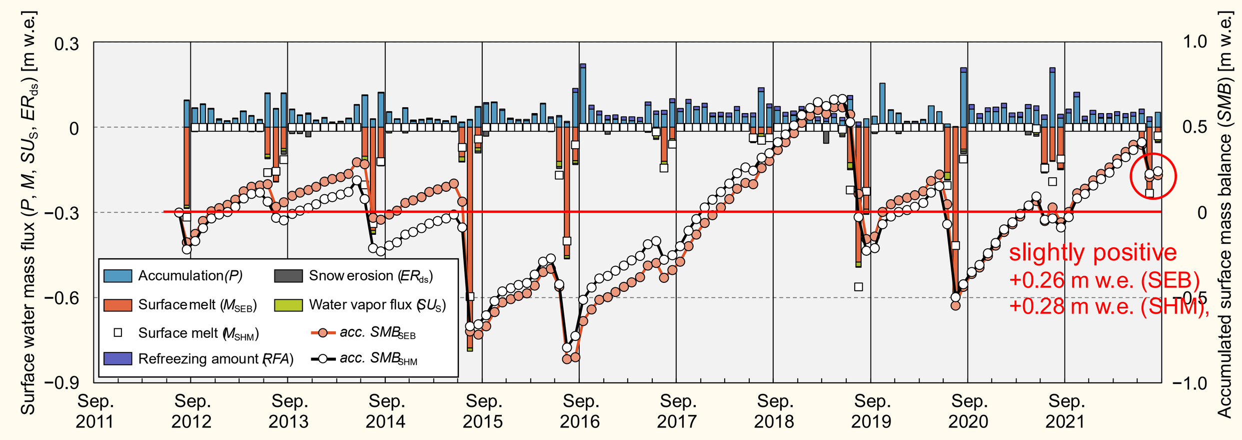

Fig. 6. Temporal variation in monthly accumulative accumulation (*P*; blue bar), surface melts (M_{SEB} and M_{SHM}; red bar and white box plot), refreezing amount (*RFA*; purple bars), water vapor flux (SU_s; green bar), and snow mass flux triggered by wind erosion (ER_{ds}; gray bar) on the left vertical axis. On the right axis, accumulative surface mass balance variations (SMB_{SEB} and SMB_{SHM}; orange and white circle plots, respectively), with zero at the start of the observation, are shown.

Observed climatology and Interannual variations of PDD and SEB

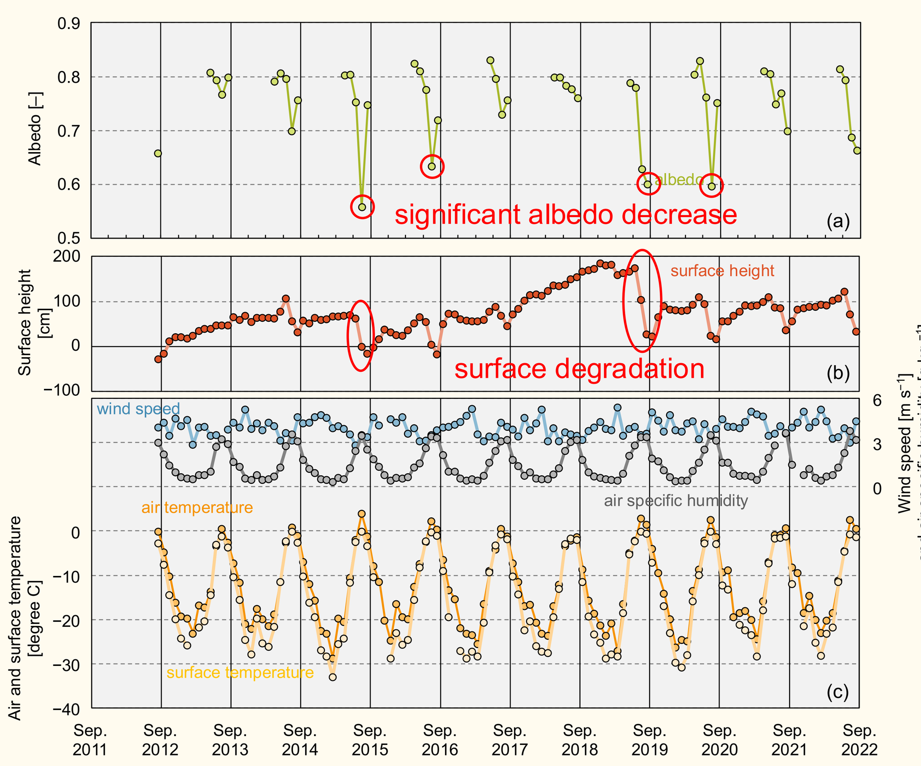

Fig. 2. Temporal variations in monthly mean (a) albedo, (b) surface height, (c) wind speed and air specific humidity, and air and surface temperatures between July 2012 and August 2022.

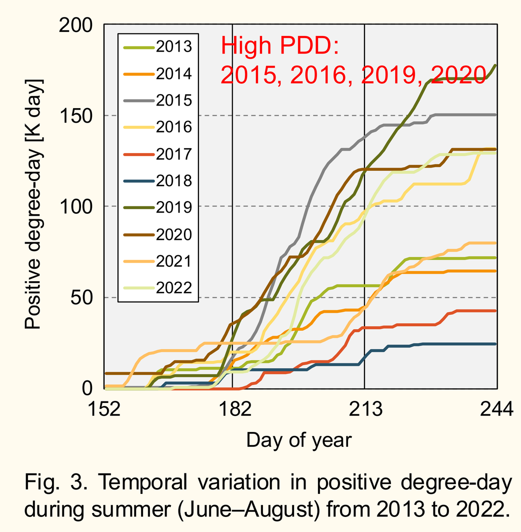

Fig. 3. Temporal variation in positive degree-day during summer (June–August) from 2013 to 2022.

A significant albedo decrease and high PDDs were recorded in 2015, 2016, 2019, and 2020 (Fig. 2a and 3). In addition, significant surface degradations were also recorded in these years (Fig. 2b; (2014/15: 144.3 cm; 2018/19: 83.9 cm). Monthly mean albedo with the lowest decrease was 0.56 in July 2015, and it was below 0.65 in summer in all other years mentioned above. Based on these results, a decrease in albedo and surface height was confirmed in these years with high air temperatures, and the trend was particularly pronounced in 2014/15 and 2018/19.

Figure 4 shows that, after April, the SW_{net} contribution to the increases in Q_{net} reached its maximum in July, when SW_{net} was 1.8 times greater than Q_{net}. This SW_{net} variation is accompanied by a similar trend of Q_{net} even though the energy components exhibit significant standard deviations in summer, particularly in July (SW_{net}: 22.8 and Q_{net}: 25.7 [W m^{-2}]).

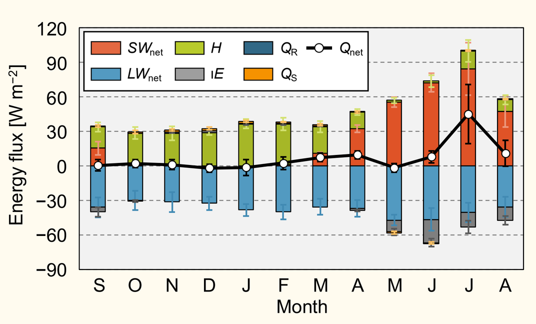

Fig. 4. Temporal variations in the 10-year averages of SW_{net}, LW_{net}, *H*, *ιE*, Q_R, Q_S, and Q_{net} for each month from 2012 to 2022. Error bars indicate ±1 standard deviation.

DISCUSSION | The causes of drastic surface melt in the 2014/15 and 2018/19 summers

High air temperatures atmospheric conditions and various radiative processes caused the melting events in the 2014/15 and 2018/19 summers (Figs. 5 and 6). These processes include the positive albedo feedback for snow and ice melting, which is caused by snow metamorphism and albedo reduction (Aoki et al., 2011) in 2014/15, as well as the cloud radiative forcing effect (Ramanathan et al., 1989) in 2018/19.

Figure 7 reveals the following features:

<2014/15 summer>

1) Low albedo and clear-sky conditions (low N_ε) were observed (JJA mean: albedo = 0.68, N_ε = 0.34).

<2018/19 summer>

1) A significant albedo decrease comparable to that observed in July 2014/15 was not observed.
2) The albedo did not increase until late August, resulting in a high monthly mean SW_{net} in August.
3) The N_ε was greater (JJA mean N_ε = 0.49), meaning that cloudy conditions were relatively continuous. This trend was most pronounced in June, where the value was 0.60.

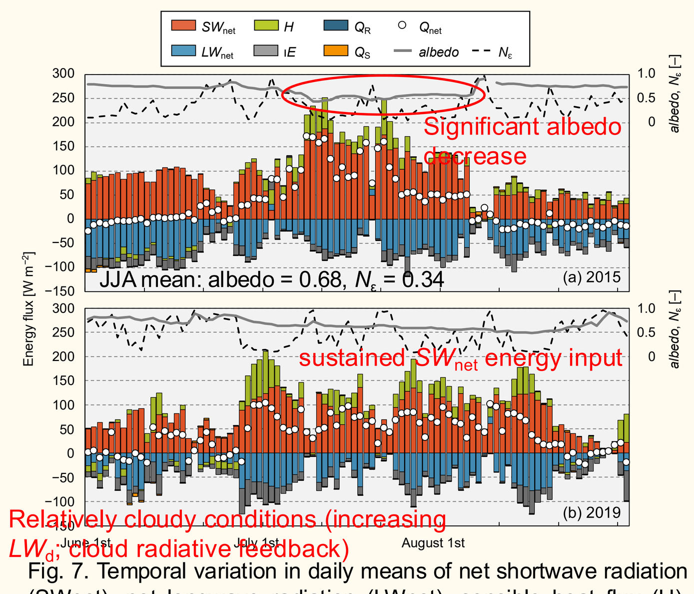

Fig. 7. Temporal variation in daily means of net shortwave radiation (SWnet), net longwave radiation (LWnet), sensible heat flux (H), latent heat flux (ιE), rainfall energy flux (QR), subsurface energy flux (QS), total of energy fluxes (Qnet), surface albedo, and cloud factor (Nε) during the summer seasons of (a) 2015 and (b) 2019.

The energy input from R_{abs} in July 2015, resulting from the SW_{net} contribution due to the snow-albedo feedback, leads to the greatest amount of surface melt. In contrast, in 2018/19 summer, the R_{abs} values remained consistently high (approximately 350 W m^{-2} or higher), resulting from the LW_d due to the cloud radiative forcing. In addition, the surface melt persisted until August 15.

Thus, the substantial SW_{net} energy input in July 2014/15 was responsible for the second-largest surface melt event, and the sustained R_{abs} energy input in the summer of 2018/19 resulted in the highest recorded amount of surface melt during the observation period.

	Total melt days [days]			
	June	Jul.	Aug.	JJA
2011/12	0	11	7	18
2012/13	3	6	6	15
2013/14	4	20	7	31
2014/15	2	22	0	24
2015/16	3	17	6	26
2016/17	0	5	8	13
2017/18	2	3	4	9
2018/19	9	24	11	44
2019/20	5	25	2	32
2020/21	2	8	11	21
2021/22	3	12	8	23

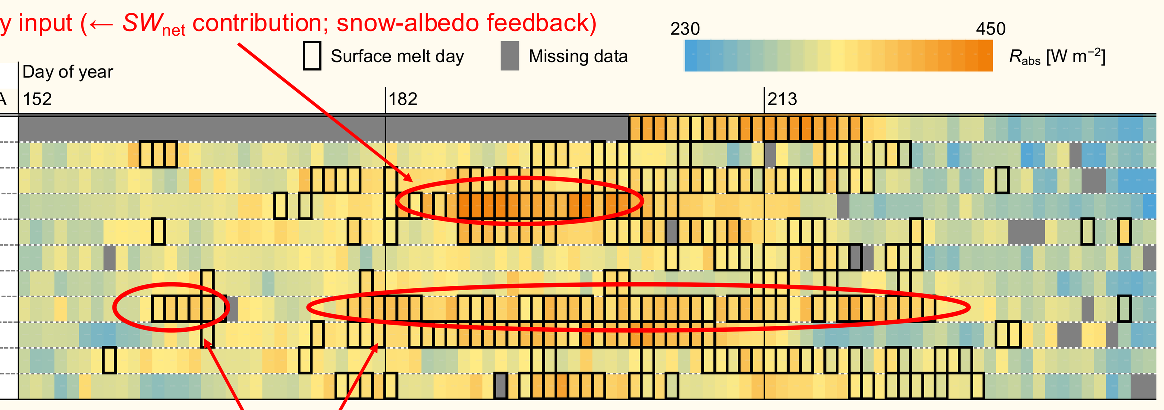

Fig. 8. Number of surface melt days defined as a daily mean surface temperature of 0° C, its distribution, and the amount of radiation absorbed by the surface (Rabs [W m^{-2}]: a sum of SW_{net} and εLW_d) in each summer (June–August). The color map indicates the R_{abs} amount, the gray areas indicate days with missing data, and the black grid lines represent surface melt days.

OUTLOOK

Increasing air temperatures in the cryosphere, as typified by "Arctic Amplification", have brought about various environmental changes, such as a decrease in albedo and changes in precipitation phase (snow to rain). Less snowfall leads the reduction in the firn layer resulting in significant mass loss in the peripheral regions of the ice sheet, where the water retention capacity is diminishing and unable to store meltwater and rainwater (Noël et al., 2017, 2022).

Should this warming trend persist in the future, mass loss may accelerate in the mid-elevation zones of coastal ice caps, such as in the vicinity of the SIGMA-B site. As demonstrated by our results, in years when significant surface melting occurred, such as in 2014/15 and 2018/19, there was a significant reduction in albedo (possibly due to ice surface exposure) at the SIGMA-B site, which is located near the ELA. In that case, the ice surface below the firn layer would be more exposed, and the results of this study suggest that, if "Arctic Amplification" continues, mass loss will accelerate as it occurred in 2014/15 and 2018/19.

SITE DESCRIPTION & METHOD

AWS site description

SIGMA-B site: On the Qaanaaq Ice Cap
(N77.518°, W69.062°: 944 m a.s.l.)
Period: July 2012 – August 2024

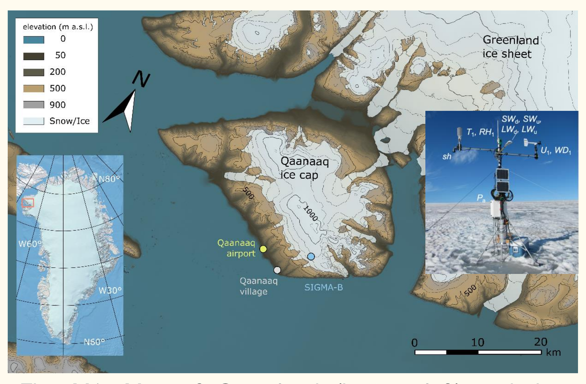

Fig. M1. Map of Greenland (bottom left) and the location of the SIGMA-B site (main map), and an overview of the AWS system at the SIGMA-B site in July 2012 (middle right). The map contour intervals of the thick and thin lines in the main map are set as 500 and 100 m a.s.l., respectively.

SEB and SMB analysis method

Surface energy balance (SEB, Q_{net}) was calculated using the observation data at the SIGMA-B site. The radiant flux absorbed by the surface (R_{abs}; Kondo and Yamazaki, 1990) is defined as the total of SW_{net} and downward longwave radiation absorbed by the surface (εLW_d). *H* and *ιE* were calculated using the bulk aerodynamic method. Surface mass balance (SMB) is defined as Eq. (1). The sign of each variable is positive for mass gain and negative for mass loss. Precipitation (*P*) is classified into P_{snow} and P_{rain}. P_{snow} is calculated using the hourly surface height (*sh*) positive change, and P_{rain} was calculated using the polar regional climate model NHM-SMAP (Niwano et al., 2018). Surface melt amount (*M*) was calculated using two methods: the surface height method (SHM), which uses the difference in hourly surface height (*sh*) data, and the SEB model. *RFA* was estimated based on each year's change in the ice surface height, identified by the surface albedo (*α*). SU_s, including four processes: sublimation, deposition, evaporation, and condensation, were calculated using the latent heat flux and surface temperature (T_s). ER_{ds} is calculated using the surface snow density and each time step difference in the surface height.

N_ε is defined as Eq. (2), an indicator of cloud cover in the sky (0: clear-sky, 1: overcast), and calculated using effective, clear-sky, and overcast atmospheric emissivity values by the methodology of Konzelmann et al. (1994) and van den Broeke et al. (2004).

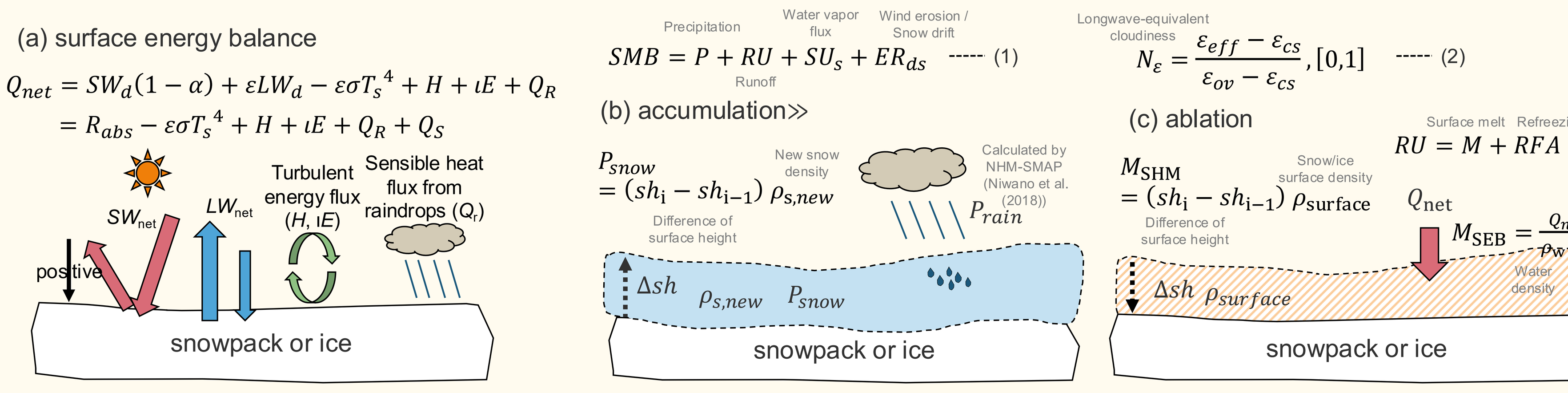

Fig. M2. Conceptual diagram of (a) the surface energy balance, (b) snow/rain accumulation, and (c) ablation by the surface energy balance model and surface height method.

≪Reference≫

Aoki, T. et al. (2011). Journal of Geophysical Research Atmospheres, 116(11), 1–22. https://doi.org/10.1029/2010JD015507
Kondo, J. and Yamazaki, T. (1990). Journal of Applied Meteorology, 29, 375–384. https://doi.org/https://doi.org/10.1175/1520-0450(1990)029<0375:APMFSS>2.0.CO;2
Konzelmann, T. et al. (1994). Global and Planetary Change, 9(1–2), 143–164. https://doi.org/10.1016/0921-8181(94)90013-2
Mouginot, J. et al. (2019). Proceedings of the National Academy of Sciences of the United States of America, 116(19), 9239–9244. https://doi.org/10.1073/pnas.1904242116
Niwano, M. et al. (2018). The Cryosphere, 12(2), 635–655. https://doi.org/10.5194/tc-12-635-2018
Noël, B. et al. (2017). Nature Communications, 8(14730). https://doi.org/10.1038/ncomms14730
Noël, B. et al. (2022). Nature Communications, 13(6870), 1–10. https://doi.org/10.1038/s41467-022-34524-x
Ramanathan, V. et al. (1989). Science, 243(4887), 57–63. https://doi.org/10.1126/science.243.4887.57
Sugiyama, S. et al. (2021). Polar Science, 27(100632). https://doi.org/10.1016/j.polar.2020.100632
Tsutaki, S. et al. (2017). Annals of Glaciology, 58(75), 181–192. https://doi.org/10.1017/aog.2017.7
van den Broeke, M. et al. (2004). Journal of Geophysical Research: Atmospheres, 109(D09103), 1–17. https://doi.org/10.1029/2003JD004394